

# BRICKSIM: A Physics-Based Simulator for Manipulating Interlocking Brick Assemblies

Haowei Wen, Ruixuan Liu, Weiyi Piao, Siyu Li, and Changliu Liu  
Robotics Institute, Carnegie Mellon University

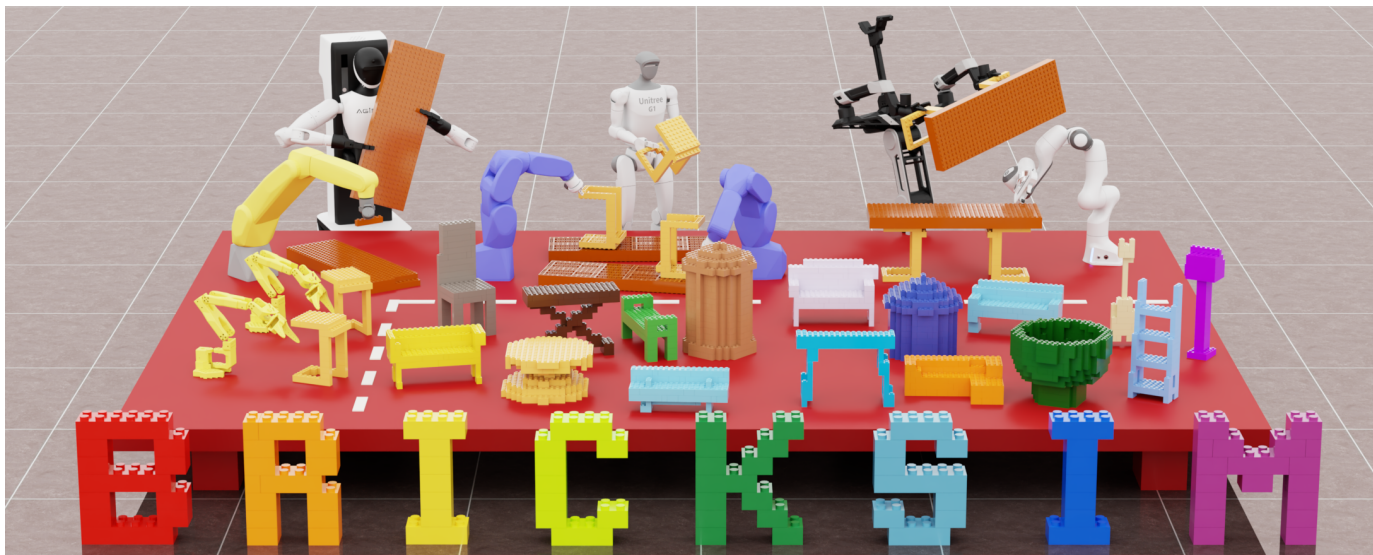


Fig. 1: **BRICKSIM Overview.** BRICKSIM enables high-fidelity simulation of complex brick assembly tasks and seamless integration with diverse robotic platforms. This teaser shows a representative multi-robot workflow for building a brick table alongside a gallery of diverse brick structures. All robotic and structural assets are natively instantiated within the BRICKSIM environment, arranged here for illustrative purposes.

**Abstract**—Interlocking brick assemblies provide a standardized yet challenging testbed for contact-rich and long-horizon robotic manipulation, but existing rigid-body simulators do not faithfully capture snap-fit mechanics. We present BRICKSIM, the first real-time physics-based simulator for interlocking brick assemblies. BRICKSIM introduces a compact force-based mechanics model for snap-fit connections and solves the resulting internal force distribution using a structured convex quadratic program. Combined with a hybrid architecture that delegates rigid-body dynamics to the underlying physics engine while handling snap-fit mechanics separately, BRICKSIM enables real-time, high-fidelity simulation of assembly, disassembly, and structural collapse. On 150 real-world assemblies, BRICKSIM achieves 100% accuracy in static stability prediction with an average solve time of 5 ms. In dynamic drop tests, it also faithfully reproduces real-world structural collapse, precisely mirroring both the occurrence of breakage and the specific breakage locations. Built on Isaac Sim, BRICKSIM further supports seamless integration with a wide variety of robots and existing pipelines. We demonstrate robotic construction of brick assemblies using BRICKSIM, highlighting its potential as a foundation for research in dexterous, long-horizon robotic manipulation. BRICKSIM is open-source, and the code is available at <https://github.com/intelligent-control-lab/BrickSim>.

## I. INTRODUCTION

Brick assembly provides a compelling and widely adopted testbed for studying contact-rich manipulation [1], [2], [3], [4], long-horizon planning [5], [6], [7], and physical reasoning [8],

[9], [10], [11]. While the individual bricks are standardized, their combinatorial compositions create highly diverse assembly tasks. These tasks are particularly challenging because they tightly couple local execution and global objectives. Robots must precisely execute each snap-fit insertion and simultaneously plan ahead to achieve the final structural goal.

Physics simulators [12], [13], [14] are essential for studying such tasks at scale, as they enable the large-scale data generation required for robot learning, safe and repeatable experimentation, and support for diverse robot embodiments. Although existing simulators excel at modeling rigid-body dynamics, they often fail to accurately capture interlocking contacts arising from micro-elastic deformation and friction, such as the snap-fit connections between bricks. In the absence of physically plausible simulators, prior work on robotic brick manipulation has either focused on simplified block-stacking tasks [15], [16], [17], [18], [19], in which smooth, non-interlocking blocks limit expressiveness and task complexity, or relied on real-world data collection [2], [4], [7], which is costly and difficult to scale. These limitations call for a simulator that preserves stable assemblies, reproduces collapse and breakage under disturbances, runs in real time, and integrates easily with modern robotic manipulation pipelines.

To address this gap, we present BRICKSIM, a real-time physics-based simulator for interlocking brick assemblies.

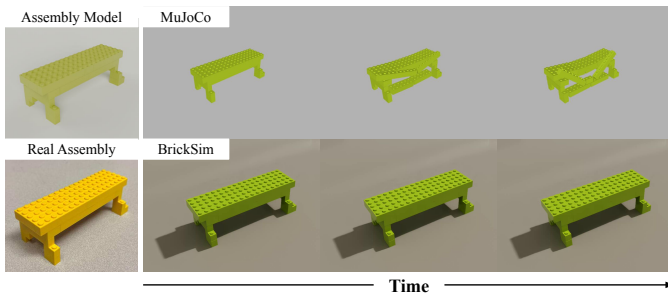


Fig. 2: Comparison of the temporal behavior of a physically stable brick assembly in MuJoCo [13] and BRICKSIM. The real assembly remains intact. Starting from the same initial state, the assembly simulated in MuJoCo progressively collapses, while BRICKSIM preserves the structure, consistent with real-world behavior.

BRICKSIM augments a general-purpose physics engine with explicit modeling of snap-fit mechanics. It detects valid stud-hole engagements to form new connections and breaks existing connections when they are overloaded. The hybrid design preserves the efficiency of the underlying physics engine while enabling accurate simulation of snap-fit connections. Built on Isaac Sim [14], BRICKSIM can be seamlessly integrated into existing robotic manipulation pipelines.

**Contributions.** Our contributions are as follows:

- We present BRICKSIM, the first real-time physics-based simulator for interlocking brick assemblies that supports physically realistic assembly, disassembly, and structural collapse, and integrates directly with Isaac Sim for robotic workflows.
- We propose a hybrid simulation architecture that handles snap-fit mechanics separately from rigid-body dynamics, allowing us to leverage both the efficiency of the underlying rigid-body physics engine and the accuracy of explicit snap-fit modeling.
- We develop a compact force-based mechanics model for snap-fit connections that yields a structured sparse convex quadratic program for internal force distribution, enabling real-time and accurate prediction of connection breakage.
- We validate BRICKSIM across both static and dynamic scenarios, achieving 100% accuracy in static stability prediction on 150 real-world assemblies, and faithfully reproducing structural collapse and breakage patterns in dynamic drop tests.

## II. RELATED WORK

We summarize a comparison of BRICKSIM with prior methods in Table I, highlighting its ability to combine physically realistic modeling, temporal dynamics, efficient runtime, and seamless robot integration.

**Brick Assembly Stability Analysis.** Determining the physical stability of a brick assembly is crucial for designing brick structures. Early work on brick assembly generation relied on heuristics to estimate constructability and optimize brick structures [20], [21], [22]. While practical, these heuristics do not provide a rigorous prediction of whether an assembly

TABLE I: Comparison of representative methods for brick assembly analysis and simulation. FSA: Force-based Stability Analysis [8], [10]. Rigid-body simulators include Gazebo [12], MuJoCo [13], and Isaac Sim [14].

	Rigid-body	FSA	BrickFEM [9]	BRICKSIM (Ours)
Snap-fit Mechanics	✗	✓	✓	✓
Temporal Dynamics	✓	✗	✓	✓
Efficient Runtime	✓	✓	✗	✓
Robot Integration	✓	✗	✗	✓

will stand or collapse. Recent efforts have inferred stability by explicitly modeling equilibrium and frictional limits, yielding more physically grounded predictions [8], [10], [23]. This improved physical understanding has benefited subsequent research on robotic brick assembly [7], [11]. Nevertheless, these methods focus primarily on static or quasi-static scenarios rather than the dynamic and temporal behaviors that arise after instability occurs. They also explicitly parameterize loads using fine-grained local force variables at contact points. Although this yields more physically grounded modeling, the resulting problem size is also larger, especially for multi-stud connections, making real-time analysis challenging.

**Physics-based Simulators.** General-purpose physics engines [12], [13], [14] simulate rigid-body dynamics quite well, but they fail to capture the snap-fit mechanics arising from micro-elastic deformation and frictional forces. Because of these modeling limitations, physically stable brick structures often collapse spontaneously in standard rigid-body simulators, as shown in Fig. 2. While recent work augments rigid-body simulators with dedicated joining models for snap-fit assembly [24], it is tailored to a specific cabinet assembly task, rather than multi-body brick assemblies with many interlocking connections and dynamically evolving topology. Closely related to our work, BrickFEM [9] uses finite element methods to predict the physical stability and temporal dynamics of brick assemblies. While effective, its approach is computationally expensive, thus limiting its applicability to real-time simulation and large-scale assemblies.

## III. OVERVIEW OF BRICKSIM

**Simulator Interface.** BRICKSIM is a ready-to-use simulator for robotic manipulation of interlocking brick assemblies. It inherits Isaac Sim’s support for robotic platform integration, rigid-body simulation, and rendering. As shown on the left of Fig. 3, users can configure both robotic embodiments and brick assets, including individual bricks and predefined assemblies from the StableText2Brick dataset [11]. The simulator supports direct UI interaction with bricks via drag-and-drop operations. For robotic manipulation, users can either teleoperate the robot [25] or deploy their own policies. Video demonstrations are provided in the code repository.

**Core Architecture.** As shown on the right of Fig. 3, BRICKSIM augments the Isaac Sim backbone with three modules: the *Brick Topology Graph* (BTG), the *Assembly Monitor* (ASM), and the *Breakage Detector* (BRD). The BTG stores snap-fit connectivity, maintains consistent relative poses

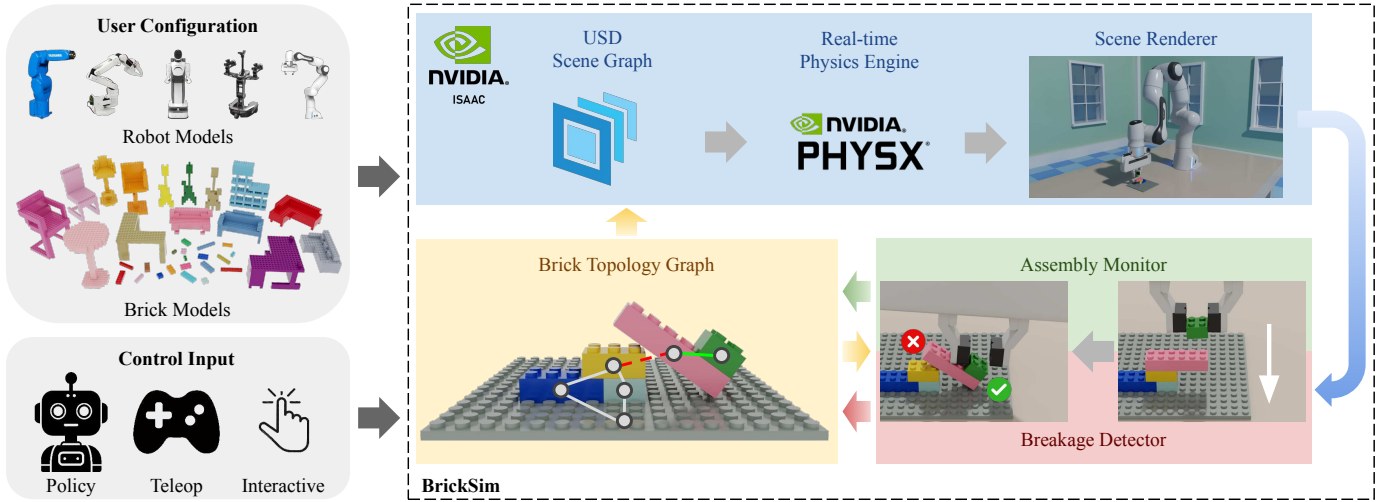


Fig. 3: **BRICKSIM Architecture.** BRICKSIM is built on top of Isaac Sim and augments its simulation stack (blue). The *Brick Topology Graph* (yellow) maintains a snap-fit connectivity graph between bricks and synchronizes it to the physics engine. The *Assembly Monitor* (green) detects valid stud-hole engagements and adds new connections, while the *Breakage Detector* (red) evaluates existing connections under external loads and removes those that fail. BRICKSIM provides a configurable simulation environment that supports diverse robotic platforms and a rich set of brick assets, including individual bricks and predefined assemblies. Bricks can be manipulated directly from the UI or by a robot controlled via teleoperation or custom policies.

of bricks within each connected component, and synchronizes rigid constraints and collision filtering with the underlying PhysX physics engine. The ASM monitors contact reports and creates new connections when two valid stud-hole engagements are detected between two bricks. The BRD evaluates the current assembly under external loads, solves for the internal force distribution, and removes overloaded connections. At each simulation step, Isaac Sim advances the rigid-body state and reports contact and impulse information. The ASM and BRD then update the topology, and the updated BTG is synchronized back to PhysX for the next step. Sec. IV details the BTG representation and its integration with the physics engine, Sec. V presents the criteria for connection formation, and Sec. VI introduces our snap-fit mechanics model, solver pipeline, and breakage criterion.

#### IV. BRICK TOPOLOGY GRAPH

We maintain a *Brick Topology Graph* (BTG) to continuously track the state of the assembly, including the specifications of each brick and the connections between them. BTG decouples the topological relationships among bricks from their physical poses in the simulator, enabling us to mitigate numerical drift introduced by the physics solver. Moreover, it allows us to leverage efficient graph-based algorithms for connectivity updates and structural reasoning.

**BTG Representation.** We represent all bricks in the scene as an undirected graph  $G = (\mathbb{V}, \mathbb{E})$ , where nodes  $\mathbb{V}$  represent bricks and edges  $\mathbb{E}$  represent kinematic connectivity. Specifically, a single edge is defined between two bricks if they are physically joined by one or more snap-fit connections. Each connected *component* in the graph corresponds to a rigidly connected assembly, and all bricks within that component have fixed relative poses with respect to one another. A rigid transform  ${}^u\mathbf{T}_v \in SE(3)$  is associated with each edge

$\{u, v\} \in \mathbb{E}$ , representing the relative pose of brick  $v$  in the frame of brick  $u$ , where  $u, v \in \mathbb{V}$ . Traversing the same edge from  $v$  to  $u$  uses the inverse transform  ${}^v\mathbf{T}_u = {}^u\mathbf{T}_v^{-1}$ . Starting from one brick, we can traverse the connected component to compute the relative pose of every brick in that component by accumulating the transforms along the path. A key invariant is that all paths between any two bricks in the same component must yield the same relative pose. We enforce this whenever a new connection is added.

**Connections.** Each brick exposes a set of *interfaces* that define admissible connection regions: a *stud* interface on the top surface and a *hole* interface on the bottom surface for cuboid bricks, as shown in Fig. 4 (a). Each interface is equipped with a local grid coordinate system aligned to brick units (unit length  $L_U = 8$  mm) and a polarity (stud vs. hole). A snap-fit *connection* is defined between a stud interface  $I_s^{(u)}$  on brick  $u$  and a hole interface  $I_h^{(v)}$  on brick  $v$ . Each connection is parameterized by a discrete tuple  $(\mathbf{o}, \psi)$ , where  $\mathbf{o} \in \mathbb{Z}^2$  is the planar grid offset in stud-grid units and  $\psi$  is the relative yaw quantized to multiples of  $\frac{\pi}{2}$ . These discrete parameters induce a rigid transform between the two interface frames.

Multiple connections may exist between the same pair of bricks, in which case all connections between them must induce the same brick-to-brick transform, and we add only one edge to the topology graph to represent their connectivity. While real  $1 \times 1$  connections allow rotation about the vertical axis, we do not allow this degree of freedom in BRICKSIM as a modeling simplification. Supporting free yaw rotation for  $1 \times 1$  connections is left for future work.

**Integration with Physics Engine.** Each brick is simulated as a rigid body with a cuboid collision proxy, as illustrated in Fig. 4 (a). We do not explicitly model stud and hole geometries in collision. Instead, snap-fit behavior is introduced

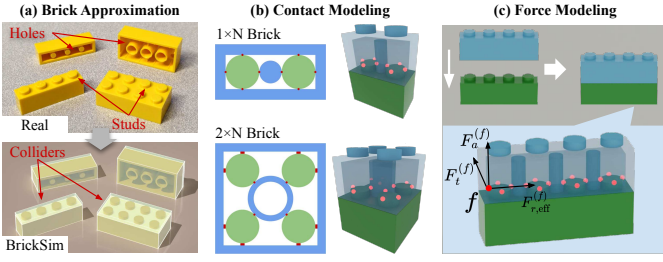


Fig. 4: **Brick and Connection Modeling.** (a) Brick geometries in the real world and the approximated collision models in BRICKSIM. (b) Depending on the dimensions of the upper brick, each stud has 3 or 4 contact points with the corresponding hole, represented as red spheres. (c) Bricks are assembled by inserting the studs of the lower brick (green) into the holes of the upper brick (blue). At each contact point  $f$ , the contact force on the lower brick is decomposed into three components: the effective radial force  $F_{r,\text{eff}}^{(f)} = F_r^{(f)} + F_0$ , where  $F_r^{(f)}$  is the variable radial force and  $F_0$  is the preload force due to snap-fit, together with the axial component  $F_a^{(f)}$  and the tangential component  $F_t^{(f)}$  of the static friction force which resist separation and twisting.

by explicitly checking for stud-hole engagement in Sec. V and adding rigid constraints to the physics engine.

For all bricks within the same connected component, we add rigid constraints to fix their relative poses according to the BTG, and we disable collision checking between them to improve simulation performance. Physics engines often struggle to propagate forces efficiently through long chains of connected bodies due to the large diameter of the constraint graph. Inspired by prior work that accelerates convergence of general articulations by adding additional long-range constraints [26], we use a simpler approach tailored to purely rigidly connected bodies. Specifically, we add extra rigid constraints between non-adjacent bricks within the same connected component, which create force-propagation shortcuts that drastically reduce the diameter of the constraint graph. We sample these extra constraints from a random regular graph with a fixed degree  $d$  (using a fixed seed for determinism) to keep the number of constraints per brick bounded, thus maintaining computational efficiency.

## V. ASSEMBLY MONITOR

Off-the-shelf rigid-body engines [12], [13], [14] do not model snap-fit mechanics. To enable snap-fit assembly, we implement an *Assembly Monitor* (ASM) that runs at every simulation step to decide when two bricks should be connected based on contact reports. At a high level, it (1) enumerates candidate brick pairs from contacts, (2) checks the geometric and force feasibility of each candidate connection, and (3) commits the accepted connections to the BTG.

**Candidate Generation.** For each simulation step, we collect brick pairs that the physics engine reports to be in contact. We then enumerate compatible stud-hole interface pairs as candidates. For cuboid bricks, this corresponds to the stud interface on the top of the lower brick and a hole interface at the bottom of the upper brick.

**Geometric Criteria.** A valid snap-fit connection must align with the discrete stud grid and have positive overlap. Given

a candidate stud interface  $I_s^{(u)}$  on brick  $u$  and hole interface  $I_h^{(v)}$  on brick  $v$ , we compute their relative pose:

$$I_s^{(u)} \mathbf{T}_{I_h^{(v)}} = \begin{bmatrix} \mathbf{R} & \mathbf{t} \\ \mathbf{0}^\top & 1 \end{bmatrix}, \quad \mathbf{t} = [t_x \quad t_y \quad t_z]^\top, \quad (1)$$

where  $\mathbf{R} \in SO(3)$  is the rotation matrix and  $\mathbf{t} \in \mathbb{R}^3$  is the translation vector. We then snap this relative pose to the nearest discrete configuration  $(\mathbf{o}, \psi)$ :

$$\mathbf{o} = \text{round} \left( \frac{1}{LU} \begin{bmatrix} t_x \\ t_y \end{bmatrix} \right), \quad \psi = \frac{\pi}{2} \text{round} \left( \frac{\theta_{\text{yaw}}}{\pi/2} \right), \quad (2)$$

where  $\theta_{\text{yaw}}$  is the relative yaw angle extracted from  $\mathbf{R}$ . We accept a candidate only if the snapped configuration is within a set of tunable geometric tolerances  $(\epsilon_z, \epsilon_{\text{tilt}}, \epsilon_\psi, \epsilon_{xy})$ :

- **Vertical distance:**  $|t_z - H_S| \leq \epsilon_z$ , where  $H_S = 1.7$  mm is the pre-engagement height implied by our collision model.
- **Tilt:**  $\theta_{\text{tilt}} \leq \epsilon_{\text{tilt}}$ , where  $\theta_{\text{tilt}}$  is the angle between the two interface normals.
- **Yaw error:**  $|\theta_{\text{yaw}} - \psi| \leq \epsilon_\psi$ .
- **Planar error:**  $\|[t_x, t_y]^\top - LU\mathbf{o}\| \leq \epsilon_{xy}$ .
- **Positive overlap:** under  $(\mathbf{o}, \psi)$ , the stud grid of  $I_s^{(u)}$  and the hole grid of  $I_h^{(v)}$  overlap with positive area.

**Force Criteria.** Geometric alignment alone is insufficient because a real snap-fit requires a pressing force to engage. We therefore gate assembly using a minimum compressive load along the stud-engagement axis. Concretely, we read the normal contact impulse between the two bricks over the simulation step from the physics engine and convert it to an average force by dividing by the step duration  $\Delta t$ . We then project this force onto the stud interface normal direction and require the resulting compressive force to exceed a fixed threshold  $F_{\text{asm}}$ .

**Connection Creation.** When a candidate satisfies both geometric and force criteria, the ASM emits a new connection  $(I_s^{(u)}, I_h^{(v)}, \mathbf{o}, \psi)$ . The BTG then inserts the connection and updates the connected components as described in Sec. IV, creating new rigid constraints and setting up collision filtering. To improve stability during assembly, we snap the bricks to the exact discrete relative transform implied by  $(\mathbf{o}, \psi)$ .

## VI. BREAKAGE DETECTOR

Real snap-fit connections can fail when overloaded, leading to disassembly or structural collapse. We model this behavior by implementing a *Breakage Detector* (BRD) that runs at every simulation step. For each connected component in the BTG, the BRD (1) builds a force-distribution optimization problem whenever the topology changes, (2) solves for the internal wrenches implied by per-brick motion and external impulses at every simulation step, and (3) breaks connections whose predicted loads exceed their frictional capacities.

### A. Constraint Model

Bricks in the same connected component are held together by two kinds of load-bearing constraints: *contacts*  $\mathbb{C}$  and *connections*  $\mathbb{K}$ . Each constraint involves two bricks and induces action-reaction wrenches on them.

**Contacts.** Contacts arise from touching brick surfaces and therefore transmit only compression. Within a connected component, the BTG fixes the relative poses of all bricks, so we compute internal contacts directly from the topology-implied brick geometry without querying the physics engine.

For the contact  $c \in \mathbb{C}$  between bricks  $i$  and  $j$ , the contact manifold  $\Omega_c$  is the convex polygonal overlap between the two surfaces. We model the contact pair as unilateral frictionless normal forces applied at the vertices of  $\Omega_c$ :

$$\lambda_c = [\lambda_c^{(v)}]_{v \in \text{Vtx}(\Omega_c)}, \quad \lambda_c^{(v)} \geq 0 \quad \forall v \in \text{Vtx}(\Omega_c), \quad (3)$$

where  $\lambda_c^{(v)}$  is the normal force at vertex  $v$  to be solved for.

The resulting wrench on brick  $i$  is

$$\begin{aligned} \mathbf{F}_{i \leftarrow c} &= - \sum_{v \in \text{Vtx}(\Omega_c)} \hat{\mathbf{n}}_c \lambda_c^{(v)}, \\ \boldsymbol{\tau}_{i \leftarrow c} &= - \sum_{v \in \text{Vtx}(\Omega_c)} (\mathbf{x}_v - \mathbf{c}_i) \times \hat{\mathbf{n}}_c \lambda_c^{(v)}, \end{aligned} \quad (4)$$

where  $\hat{\mathbf{n}}_c$  is the contact normal,  $\mathbf{x}_v$  is the position of vertex  $v$ , and  $\mathbf{c}_i$  is the COM of brick  $i$ . The wrench on the other brick  $j$  follows from Newton's third law.

**Connections.** Connections arise from snap-fit engagements and can carry tension, shear, and torsion through frictional interlocking. A connection  $k \in \mathbb{K}$  includes an array of studs, and each stud has 3 or 4 contact points with the hole, depending on the dimensions of the upper brick as illustrated in Fig. 4 (b) [8], [10].

Let  $\mathbb{F}_k$  denote the set of all contact points for connection  $k$ . The forces at different contact points  $f \in \mathbb{F}_k$  are not independent but are coupled by the micro-displacement between the two bricks. By exploiting this coupling, we reduce each connection to a fixed small set of decision variables, thereby reducing both the number of variables and the number of constraints in the optimization problem.

We define  $\hat{\mathbf{u}}_k, \hat{\mathbf{v}}_k, \hat{\mathbf{n}}_k$  as the orthonormal basis of the connection frame, where  $\hat{\mathbf{n}}_k$  points upward along the stud axis. We capture the aforementioned coupling by modeling the traction components along  $\hat{\mathbf{n}}_k, \hat{\mathbf{u}}_k, \hat{\mathbf{v}}_k$  as three affine fields evaluated at each contact point  $f \in \mathbb{F}_k$  located at  $(u_f, v_f)$  in the connection frame:

$$p_{k,n}^{(f)} = \phi_f^\top \boldsymbol{\alpha}_k, \quad p_{k,u}^{(f)} = \phi_f^\top \boldsymbol{\beta}_k, \quad p_{k,v}^{(f)} = \phi_f^\top \boldsymbol{\gamma}_k, \quad (5)$$

where  $\phi_f = [1 \ u_f \ v_f]^\top$ , and  $\boldsymbol{\alpha}_k, \boldsymbol{\beta}_k, \boldsymbol{\gamma}_k \in \mathbb{R}^3$  are unknown coefficients to be solved for.

Let  $\mathbf{n}_f$  be the inward radial normal of the stud at contact point  $f$ , and  $\mathbf{t}_f = \hat{\mathbf{n}}_k \times \mathbf{n}_f$  be the tangential direction. As illustrated in Fig. 4 (c), the force at  $f$  can be decomposed into

an axial component  $F_a^{(f)}$  along  $\hat{\mathbf{n}}_k$ , a radial component  $F_r^{(f)}$  along  $\mathbf{n}_f$ , and a tangential component  $F_t^{(f)}$  along  $\mathbf{t}_f$ :

$$\begin{aligned} F_a^{(f)} &= p_{k,n}^{(f)}, \\ F_r^{(f)} &= \mathbf{n}_f^\top (p_{k,u}^{(f)} \hat{\mathbf{u}}_k + p_{k,v}^{(f)} \hat{\mathbf{v}}_k), \\ F_t^{(f)} &= \mathbf{t}_f^\top (p_{k,u}^{(f)} \hat{\mathbf{u}}_k + p_{k,v}^{(f)} \hat{\mathbf{v}}_k), \end{aligned} \quad (6)$$

which are linear in the affine field coefficients. The resulting wrench on  $i$  due to  $f$  is then

$$\begin{aligned} \mathbf{F}_{i \leftarrow f} &= \hat{\mathbf{n}}_k \phi_f^\top \boldsymbol{\alpha}_k + \hat{\mathbf{u}}_k \phi_f^\top \boldsymbol{\beta}_k + \hat{\mathbf{v}}_k \phi_f^\top \boldsymbol{\gamma}_k, \\ \boldsymbol{\tau}_{i \leftarrow f} &= (\mathbf{x}_f - \mathbf{c}_i) \times \mathbf{F}_{i \leftarrow f}, \end{aligned} \quad (7)$$

where  $\mathbf{x}_f$  is the position of contact point  $f$ . Summing over  $f \in \mathbb{F}_k$  gives the total wrench  $\mathbf{F}_{i \leftarrow k}$  and  $\boldsymbol{\tau}_{i \leftarrow k}$  in linear form in  $\boldsymbol{\alpha}_k, \boldsymbol{\beta}_k, \boldsymbol{\gamma}_k$ .

In our model, stud and hole interfaces lie on the surfaces of the bricks, so every connection is co-located with a contact that carries compression, and we therefore explicitly constrain  $F_a^{(f)}$  to be tension-only:

$$F_a^{(f)} \geq 0 \quad \forall f \in \mathbb{F}_k. \quad (8)$$

Let  $F_0$  denote the preload force resulting from the micro-elastic deformation of the stud and hole due to snap-fit. Then the effective normal force at  $f$  is  $F_{r,\text{eff}}^{(f)} = F_r^{(f)} + F_0$ . The axial and tangential forces are limited by friction, and we approximate the friction cone with a linear friction pyramid:

$$|F_t^{(f)}| + F_a^{(f)} \leq \mu F_{r,\text{eff}}^{(f)} \quad \forall f \in \mathbb{F}_k, \quad (9)$$

where  $\mu$  is the static friction coefficient for ABS plastic. While the actual friction limit depends on the manufacturing tolerance and wear of the bricks, we use the typical values  $\mu = 0.2$  and  $\mu F_0 = 0.7 \text{ N}$  [8].

### B. Solving Force Distribution

**Equilibrium Equations.** To solve for the internal forces, we compute the net internal wrench  $\mathbf{b}_i \in \mathbb{R}^6$  required on brick  $i$  from the physics engine's outputs:

$$\mathbf{b}_i = \frac{1}{\Delta t} \left( \left[ \begin{array}{c} m_i (\mathbf{v}_i^+ - \mathbf{v}_i^-) \\ \mathbf{I}_i^+ \boldsymbol{\omega}_i^+ - \mathbf{I}_i^- \boldsymbol{\omega}_i^- \end{array} \right] - \left[ \begin{array}{c} \mathbf{J}_i^{\text{ext}} \\ \mathbf{H}_i^{\text{ext}} \end{array} \right] \right), \quad (10)$$

where  $\Delta t$  is the simulation step duration,  $m_i$  is the brick mass,  $\mathbf{v}_i^\pm, \boldsymbol{\omega}_i^\pm$  and  $\mathbf{I}_i^\pm$  are the brick's COM twist and inertia tensor before and after the simulation step, and  $\mathbf{J}_i^{\text{ext}}, \mathbf{H}_i^{\text{ext}}$  are the external impulses (including gravity). Stacking all unknowns in (3) and (5) into a decision variable  $\mathbf{x}$ , the equilibrium can be written as a linear system:

$$\sum_{c \in \mathbb{C}_i \cup \mathbb{K}_i} \begin{bmatrix} \mathbf{F}_{i \leftarrow c} \\ \boldsymbol{\tau}_{i \leftarrow c} \end{bmatrix} = \mathbf{b}_i \quad \forall i \in \mathbb{V}_c \iff \mathbf{A} \mathbf{x} = \mathbf{b}, \quad (11)$$

where  $\mathbb{C}_i$  and  $\mathbb{K}_i$  are the constraints involving brick  $i$ ,  $\mathbb{V}_c \subseteq \mathbb{V}$  is the current connected component,  $\mathbf{A}$  is the equilibrium matrix that depends only on the topology and geometry of the assembly, and  $\mathbf{b}$  stacks all  $\mathbf{b}_i$ .

Enforcing the non-negativity constraints in (3) and (8), and the friction constraints in (9) at the vertices of the contact and connection boundaries gives linear inequalities:

$$\mathbf{G}\mathbf{x} \geq \mathbf{0}, \quad \mathbf{H}\mathbf{x} \leq \mathbf{1}. \quad (12)$$

**Robust Quadratic Programming.** To select a physically plausible force distribution among feasible solutions, we minimize an elastic-energy surrogate:

$$U_f = \frac{1}{2} \left[ w_a (F_a^{(f)})^2 + w_r (F_r^{(f)})^2 + w_t (F_t^{(f)})^2 \right], \quad (13)$$

$$U = \sum_{k \in \mathbb{K}} \sum_{f \in \mathbb{F}_k} U_f = \frac{1}{2} \mathbf{x}^\top \mathbf{Q} \mathbf{x},$$

where  $w_a, w_r, w_t$  are compliance weights, and  $\mathbf{Q}$  is a quadratic form, which leads to a convex sparse quadratic program (QP).

However, the formulation above comes with two challenges in practice. First, the system  $\mathbf{A}\mathbf{x} = \mathbf{b}$  may not have a solution when  $\mathbf{b} \notin \text{colsp}(\mathbf{A})$  due to degenerate geometries and numerical drifts from the physics engine. Second, the hard friction constraints make the QP infeasible when a connection is overloaded, yielding no solution and thus no failure diagnosis.

We therefore use a robust, lexicographic relaxation to solve the problem in three stages, all of which are convex sparse QPs. The three sequential QPs are formulated as follows:

- 1) Project  $\mathbf{b}$  to the feasible subspace:

$$\begin{aligned} \mathbf{b}^* &= \underset{\mathbf{y}}{\text{argmin}} \|\mathbf{y} - \mathbf{b}\|^2 \\ \text{s.t.} \quad \exists \mathbf{x} \quad \mathbf{A}\mathbf{x} &= \mathbf{y}, \quad \mathbf{G}\mathbf{x} \geq \mathbf{0}. \end{aligned} \quad (14)$$

- 2) Find the minimum friction-feasibility relaxation  $\mathbf{v}^*$ :

$$\begin{aligned} \mathbf{v}^* &= \underset{\mathbf{v}}{\text{argmin}} \|\mathbf{v}\|^2 \\ \text{s.t.} \quad \exists \mathbf{x} \quad \mathbf{A}\mathbf{x} &= \mathbf{b}^*, \quad \mathbf{G}\mathbf{x} \geq \mathbf{0}, \\ \mathbf{H}\mathbf{x} &\leq \mathbf{1} + \mathbf{S}\mathbf{v}, \quad \mathbf{v} \geq \mathbf{0}, \end{aligned} \quad (15)$$

where  $\mathbf{v} = [v_k]_{k \in \mathbb{K}}$  is a per-connection relaxation and  $\mathbf{S}$  maps  $v_k$  to the corresponding friction rows.

- 3) Minimize the objective in (13) under the relaxed constraints:

$$\begin{aligned} \mathbf{x}^* &= \underset{\mathbf{x}}{\text{argmin}} \frac{1}{2} \mathbf{x}^\top \mathbf{Q} \mathbf{x} \\ \text{s.t.} \quad \mathbf{A}\mathbf{x} &= \mathbf{b}^*, \quad \mathbf{G}\mathbf{x} \geq \mathbf{0}, \quad \mathbf{H}\mathbf{x} \leq \mathbf{1} + \mathbf{S}\mathbf{v}^*. \end{aligned} \quad (16)$$

Crucially, all quantities used by the BRD are expressed in a connected-component frame attached to the BTG. Because all bricks in a connected component have fixed relative poses in this frame, as long as the assembly topology remains unchanged, all cost and constraint matrices remain constant, and only the right-hand side vectors update at each simulation step. This specific structure is well suited to the OSQP solver [27], which caches matrix factorizations and warm-starts from the previous solution, allowing the breakage detector to run in real time.

TABLE II: **Comparison of Static Structural Stability Analysis.** Stability analysis results on 150 brick assemblies. Ground-truth stability is established by building each structure in reality. Accuracy and average solve time are computed over solvable structures only.

	BrickFEM [9]	StableLEGO [10]	Ours
Solvable Count	98	<b>150</b>	<b>150</b>
Solvability	65.3%	<b>100%</b>	<b>100%</b>
False-Stable Count	22	0	0
False-Unstable Count	0	3	0
Physical Accuracy	77.6%	98%	<b>100%</b>
Avg. Solve Time (s)	193.9	0.027	<b>0.005</b>

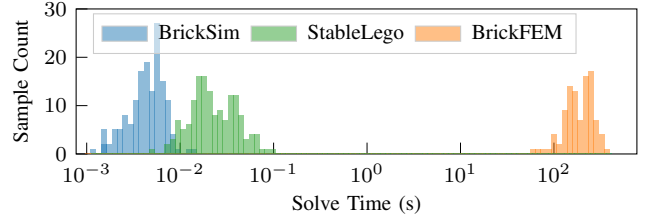


Fig. 5: **Comparison of Solve Time.** Distributions of computation times for static structural stability analysis over all solvable structures.

### C. Breakage Criterion

After solving the aforementioned QP problem, we compute a per-connection utilization score  $u_k$  based on the solved force distribution  $\mathbf{x}^*$ :

$$u_k = \max_{f \in \mathbb{F}_k} \frac{|F_t^{(f)}| + F_a^{(f)}}{\mu(F_r^{(f)} + F_0)}, \quad (17)$$

where  $u_k > 1$  indicates that the connection is overloaded and likely to break.

Although multiple connections may satisfy  $u_k > 1$ , breaking all of them at once would be overly aggressive and non-physical. We therefore identify the most offending connection and break the smallest number of overloaded connections containing it whose removal disconnects the connected component. Applying this procedure at every simulation step mimics the progressive breakage behavior observed in the real world.

## VII. RESULTS

We conduct a comprehensive set of experiments to evaluate the simulation performance of BRICKSIM. Specifically, we (1) analyze its ability to assess structural stability in static brick assemblies, (2) evaluate its performance in simulating dynamic assembly processes, and (3) demonstrate its effectiveness in supporting robotic manipulation tasks within BRICKSIM. All experiments are conducted on a machine equipped with an Intel i9-12900H CPU, 64 GB of RAM, and an NVIDIA RTX 3080 Ti Mobile GPU. Unless otherwise specified, the following parameters are used:  $\epsilon_z = 1.0$  mm,  $\epsilon_{\text{tilt}} = 5^\circ$ ,  $\epsilon_\psi = 5^\circ$ ,  $\epsilon_{xy} = 2.0$  mm,  $F_{\text{asm}} = 1.0$  N,  $w_a = w_r = w_t = 1.0$ , and  $d = 4$ .

### A. Static Stability Evaluation

We compare the static structural stability predicted by BRICKSIM with two representative baselines: BrickFEM [9]

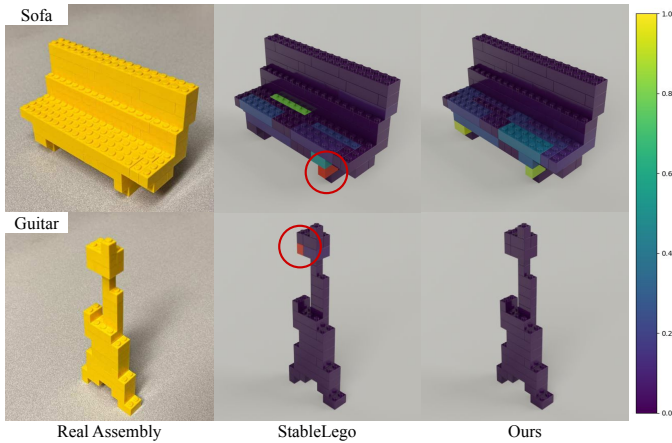


Fig. 6: **Comparison of Predicted Force Distributions.** Stress values range from 0 to 1, where lower values indicate smaller internal stress and higher values indicate greater stress, suggesting a higher risk of structural failure. Red: predicted collapsing bricks.

and StableLego [10]. The evaluation set is randomly sampled from StableText2Brick [11] and consists of 150 assemblies with up to 30 bricks. Ground-truth stability is established by physically building each assembly and observing whether it collapses without external support.

As shown in Table II, BRICKSIM and StableLego both achieve 100% solvability, whereas BrickFEM frequently fails due to errors or exceeding the 20-minute time limit. BRICKSIM achieves perfect 100% accuracy, demonstrating its strong physical fidelity. StableLego exhibits a conservative tendency, with all of its incorrect predictions being false-unstable. BrickFEM, on the other hand, misclassifies over 20 unstable structures as stable. Fig. 6 shows two failure cases of StableLego. Although StableLego and BRICKSIM both produce similar internal force patterns on most bricks, StableLego significantly overestimates the internal stresses on certain bricks, as highlighted in red, leading to incorrect predictions of unstable structures. This comparison further demonstrates the improved physical correctness of BRICKSIM in modeling interlocking snap-fit connections.

In addition to physical correctness, we compare the average solve times in Table II. BRICKSIM achieves the lowest average solve time, significantly outperforming the baselines. Fig. 5 illustrates the distribution of solve times for each method. In general, BrickFEM requires several hundred seconds per structure, whereas StableLego takes approximately 10 ms to 100 ms. BRICKSIM, in contrast, only takes around 1 ms to 10 ms, which is an order of magnitude faster than StableLego and four orders of magnitude faster than BrickFEM. By reducing computation time to the millisecond scale, BRICKSIM overcomes the stability analysis bottleneck, making end-to-end real-time simulation computationally feasible.

### B. Dynamic Structure Simulation

Beyond static structures, we evaluate the physical fidelity of BRICKSIM in capturing temporal dynamics and structural failure. Specifically, we perform controlled drop tests in which

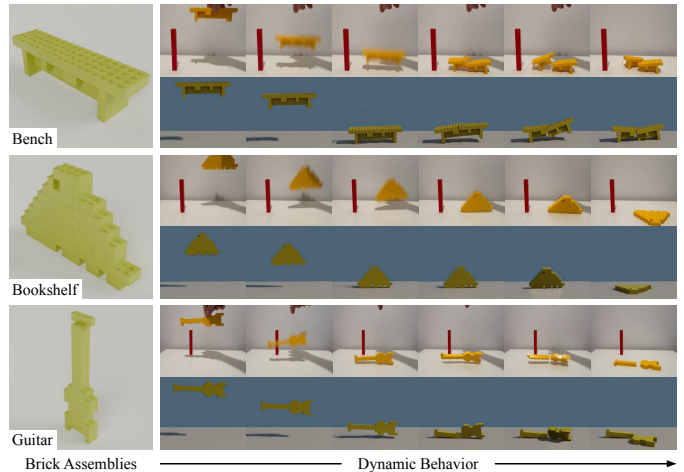


Fig. 7: **Comparison of Temporal Dynamics.** We compare the real and simulated behaviors of three brick assemblies dropped from midair. Top row: real observations. Bottom row: simulated motions from BRICKSIM.

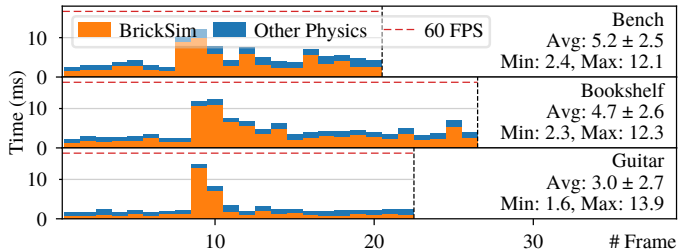


Fig. 8: **End-to-End Frame Time in Drop Tests.** We measure the per-frame computation time for the three drop test simulations. Each stacked bar corresponds to one simulation frame and is decomposed into time spent in BRICKSIM and “Other Physics” (the remaining physics computation handled by Isaac Sim). The red dashed line marks the 60 FPS budget of 16.7 ms. Annotations report total frame times (avg  $\pm$  std, min, max).

brick assemblies are released from a height of approximately 15 bricks (indicated by the red stick in Fig. 7) and impact a rigid table. We record the real-world behaviors and compare them against the dynamics simulated by BRICKSIM. Upon impact, the real-world bookshelf remains intact, and BRICKSIM successfully simulates its strong interlocking connections. In contrast, the bench and guitar split into two pieces upon collision. BRICKSIM correctly simulates their structural collapse, despite minor differences in the motions of the split components after breakage. Moreover, BRICKSIM precisely mirrors the specific breakage locations observed in the real-world experiments. These results demonstrate the strong physical fidelity of BRICKSIM in modeling the temporal dynamics of brick assemblies.

Additionally, we measure the end-to-end frame times in the drop test simulations, as shown in Fig. 8. Across all of the three assemblies (consisting up to 30 bricks), the simulation strictly adheres to the 16.7 ms budget required for 60 FPS. While frame times briefly peak during breakage due to BTG updates, they still remain below the real-time threshold, and the vast majority of frames process in under 10 ms. These results demonstrate that BRICKSIM successfully maintains

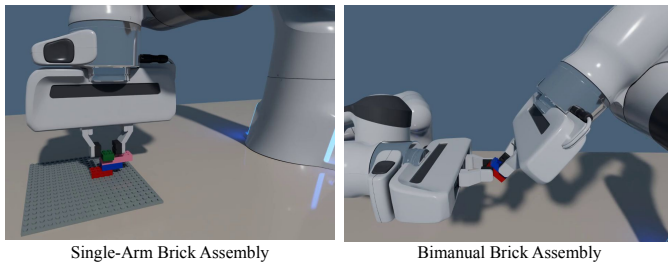


Fig. 9: **Robotic Brick Manipulation using BRICKSIM.** Left: a Franka robot is building an assembly by sequentially stacking bricks onto a baseplate on the table. Right: two Franka robots are cooperating to assemble two bricks in hand. One robot is holding the red brick, while the other robot is inserting the blue brick into it.

real-time performance throughout the simulation.

### C. Robotic Demonstration

We further demonstrate robot integration in Fig. 9. In the left scenario, a Franka robot stacks bricks onto a baseplate to construct an assembly. In the right scenario, two Franka robots cooperate to assemble two bricks in hand. Both demonstrations are implemented using the Python API provided by BRICKSIM and leverage Isaac Sim’s built-in robotic assets and motion-planning pipelines. Demonstration videos are provided in the code repository.

## VIII. DISCUSSION

Brick assembly provides a highly complex and diverse, yet standardized, platform for robotic manipulation research. BRICKSIM brings brick assembly into simulation, significantly lowering the barrier to entry for researchers. This accessibility promotes reproducibility, large-scale benchmarking, and rapid prototyping of algorithms in robot learning and manipulation. More broadly, BRICKSIM suggests an effective paradigm for physics simulation. Rather than implementing a task-specific simulator from scratch, one can introduce task-specific mechanics into a mature physics simulator while preserving its rich ecosystem, reliability, and efficiency. We hope BRICKSIM will foster broader collaboration across the robotics, graphics, and physics simulation communities and serve as a stepping stone toward more generalizable solutions for contact-rich, long-horizon manipulation and real-world assembly tasks.

**Limitations.** First, the frame time of BRICKSIM still grows with the structural complexity of the assembly. The current version can handle assemblies with fewer than 50 bricks while maintaining real-time performance. As assemblies grow larger and more densely connected, computational costs increase, resulting in reduced frame rates. That said, we believe the current capacity is sufficient for most existing research scenarios, as state-of-the-art robotic brick manipulation systems typically operate on assemblies with fewer than 50 bricks [28]. Improving scalability through better parallelization and more efficient solvers remains an important direction for future work. Second, BRICKSIM currently supports parts with fixed snap-fit connections, such as bricks, plates, and slopes. In future work, we aim to expand support to functional parts

such as gears and wheels, which introduce additional degrees of freedom and allow more complex interactions and dynamic behaviors.

## ACKNOWLEDGMENT

This material is based upon work supported in part by the National Science Foundation under Grant No. 2403061. The authors also thank Maggie Cai for teleoperating the robot in the demonstration video.

## REFERENCES

- [1] I. Popov et al., “Data-efficient deep reinforcement learning for dexterous manipulation,” *arXiv preprint arXiv:1704.03073*, 2017.
- [2] R. Liu, Y. Sun, and C. Liu, “A lightweight and transferable design for robust lego manipulation,” in *International Symposium on Flexible Automation (ISFA)*, 2024.
- [3] Y. Chen, C. Wang, L. Fei-Fei, and C. K. Liu, “Sequential dexterity: Chaining dexterous policies for long-horizon manipulation,” in *7th Conference on Robot Learning*, 2023.
- [4] C. Gu et al., “Manualvla: A unified vla model for chain-of-thought manual generation and robotic manipulation,” *arXiv preprint arXiv:2512.02013*, 2025.
- [5] L. Nägele, A. Hoffmann, A. Schierl, and W. Reif, “Legobot: Automated planning for coordinated multi-robot assembly of lego structures,” in *IEEE/RSJ International Conference on Intelligent Robots and Systems (IROS)*, 2020.
- [6] R. Liu, A. Chen, W. Zhao, and C. Liu, “Physics-aware combinatorial assembly sequence planning using data-free action masking,” *IEEE Robotics and Automation Letters (RA-L)*, vol. 10, no. 5, pp. 4882–4889, 2025.
- [7] P. Huang, R. Liu, S. Aggarwal, C. Liu, and J. Li, “Apex-mr: Multi-robot asynchronous planning and execution for cooperative assembly,” in *Robotics: Science and Systems (RSS)*, 2025.
- [8] S.-J. Luo et al., “Legolization: Optimizing lego designs,” *ACM Transactions on Graphics (TOG)*, vol. 34, no. 6, pp. 222:1–222:12, 2015.
- [9] M. Pletz and M. Drvoderic, “Brickfem an automated finite element model for static and dynamic simulations of simple lego sets,” *engrXiv preprint*, 2023. DOI: 10.31222/2898
- [10] R. Liu, K. Deng, Z. Wang, and C. Liu, “Stablelego: Stability analysis of block stacking assembly,” *IEEE Robotics and Automation Letters (RA-L)*, vol. 9, no. 11, pp. 9383–9390, 2024.
- [11] A. Pun, K. Deng, R. Liu, D. Ramanan, C. Liu, and J.-Y. Zhu, “Generating physically stable and buildable brick structures from text,” in *IEEE International Conference on Computer Vision (ICCV)*, 2025.
- [12] N. Koenig and A. Howard, “Design and use paradigms for gazebo, an open-source multi-robot simulator,” in *IEEE/RSJ International Conference on Intelligent Robots and Systems (IROS)*, 2004.
- [13] E. Todorov, T. Erez, and Y. Tassa, “Mujoco: A physics engine for model-based control,” in *IEEE/RSJ International Conference on Intelligent Robots and Systems (IROS)*, 2012.
- [14] NVIDIA, *Isaac Sim*, Version 5.1.0, 2025. [Online]. Available: <https://github.com/isaac-sim/IsaacSim>
- [15] O. Groth, F. B. Fuchs, I. Posner, and A. Vedaldi, “Shapestacks: Learning vision-based physical intuition for generalised object stacking,” in *European Conference on Computer Vision (ECCV)*, 2018.
- [16] V. Bapst et al., “Structured agents for physical construction,” in *International Conference on Machine Learning (ICML)*, 2019.
- [17] N. Fazeli, M. Oller, J. Wu, Z. Wu, J. B. Tenenbaum, and A. Rodriguez, “See, feel, act: Hierarchical learning for complex manipulation skills with multisensory fusion,” *Science Robotics*, vol. 4, no. 26, eaav3123, 2019.
- [18] A. Goldberg et al., “Blox-net: Generative design-for-robot-assembly using vlm supervision, physics simulation, and a robot with reset,” in *IEEE International Conference on Robotics and Automation (ICRA)*, 2025.
- [19] Y. Xu, L. Li, C. Yu, and D. Hsu, ““stack it up!”: 3d stable structure generation from 2d hand-drawn sketch,” in *9th Conference on Robot Learning*, 2025.
- [20] R. A. H. Gower, A. E. Heydtmann, and H. G. Petersen, “Lego: Automated model construction,” in *32nd European Study Group with Industry - Final Report*, 1998.

- [21] S. Ono, A. André, Y. Chang, and M. Nakajima, "Lego builder: Automatic generation of lego assembly manual from 3d polygon model," *ITE Transactions on Media Technology and Applications*, vol. 1, no. 4, pp. 354–360, 2013.
- [22] R. P. Testuz, Y. Schwartzburg, and M. Pauly, "Automatic generation of constructable brick sculptures," in *Eurographics 2013 - Short Papers*, 2013.
- [23] T. Kollsker and E. Malaguti, "Models and algorithms for optimising two-dimensional lego constructions," *European Journal of Operational Research*, vol. 289, no. 1, pp. 270–284, 2021.
- [24] A. Lämmle, Z. Xiang, and B. A. Bálint, "Extension of established modern physics simulation for the training of robotic electrical cabinet assembly," *Procedia CIRP*, vol. 107, pp. 1317–1322, 2022.
- [25] R. Cadene et al., *Lerobot: State-of-the-art machine learning for real-world robotics in pytorch*, 2024. [Online]. Available: <https://github.com/huggingface/lerobot>
- [26] M. Müller, N. Chentanez, M. Macklin, and S. Jeschke, "Long range constraints for rigid body simulations," in *Proceedings of the ACM SIGGRAPH / Eurographics Symposium on Computer Animation*, 2017.
- [27] B. Stellato, G. Banjac, P. Goulart, A. Bemporad, and S. Boyd, "Osqp: An operator splitting solver for quadratic programs," *Mathematical Programming Computation*, vol. 12, no. 4, pp. 637–672, 2020.
- [28] R. Liu et al., "Prompt-to-product: Generative assembly via bimanual manipulation," *arXiv preprint arXiv:2508.21063*, 2025.